Short Article

Cell Metabolism

Protein Kinase C Epsilon Deletion in Adipose Tissue, but Not in Liver, Improves Glucose Tolerance

Graphical Abstract

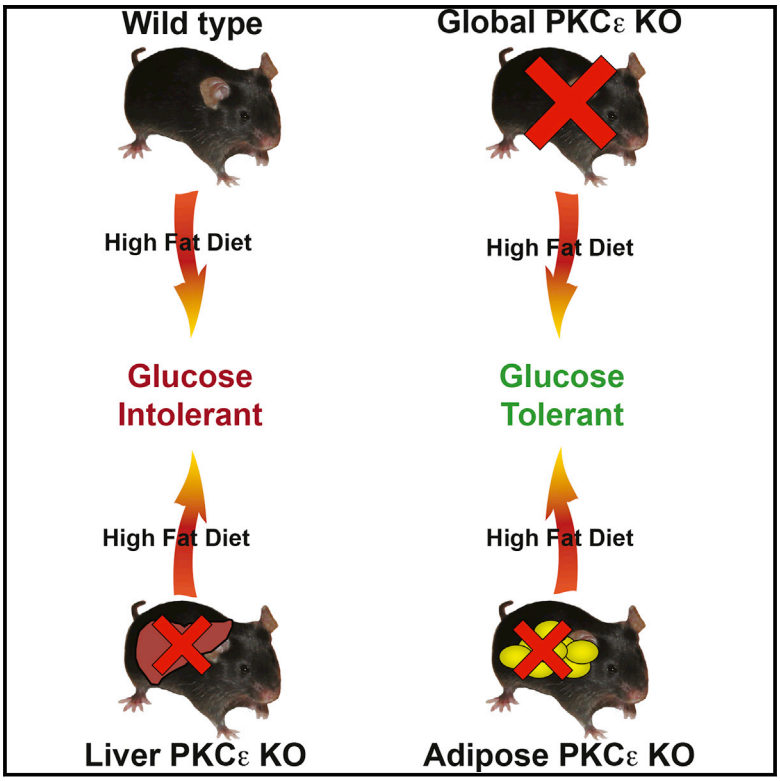

Highlights

- PKCε in liver does not mediate fat-diet-induced insulin resistance
- Adipose-tissue-specific PKCε deletion improves diet-induced glucose intolerance
- PKCε deletion does not affect the phosphorylation of insulin signaling components
- PKCε in adipose tissue affects liver gene transcription and lipid metabolism

Authors

Amanda E. Brandon, Bing M. Liao, Barbara Diakanastasis, ..., Mark A. Febbraio, Trevor J. Biden, Carsten Schmitz-Peiffer

Correspondence

c.schmitz-peiffer@garvan.org.au

In Brief

Using tissue-specific deletions of protein kinase C epsilon (PKCε) in fat-fed mice, Brandon et al. show that PKCε does not act directly in the liver to cause insulin resistance but instead acts in the adipose tissue to protect against glucose intolerance through an insulin signaling-independent mechanism.

Brandon et al., 2019, Cell Metabolism *29*, 183–191
January 8, 2019
https://doi.org/10.1016/j.cmet.2018.09.013

CellPress

Cell Metabolism
Short Article

Protein Kinase C Epsilon Deletion in Adipose Tissue, but Not in Liver, Improves Glucose Tolerance

Amanda E. Brandon,[1,2,5] Bing M. Liao,[1,5] Barbara Diakanastasis,[1,5] Benjamin L. Parker,[2] Katy Raddatz,[1] Sophie A. McManus,[1] Liam O'Reilly,[1] Erica Kimber,[1] A. Gabrielle van der Kraan,[1] Dale Hancock,[2] Darren C. Henstridge,[3] Peter J. Meikle,[3] Gregory J. Cooney,[1,2] David E. James,[2] Saskia Reibe,[1] Mark A. Febbraio,[1,4] Trevor J. Biden,[1,4] and Carsten Schmitz-Peiffer[1,4,6,*]

[1]Diabetes and Metabolism Division, Garvan Institute of Medical Research, Sydney, NSW 2010, Australia
[2]School of Life and Environmental Sciences, The University of Sydney, Sydney, NSW 2006, Australia
[3]Baker Heart and Diabetes Institute, Melbourne, VIC 3004, Australia
[4]St Vincent's Clinical School, University of New South Wales, Sydney, NSW 2010, Australia
[5]These authors contributed equally
[6]Lead Contact
*Correspondence: c.schmitz-peiffer@garvan.org.au
https://doi.org/10.1016/j.cmet.2018.09.013

SUMMARY

Protein kinase C epsilon (PKCε) activation in the liver is proposed to inhibit insulin action through phosphorylation of the insulin receptor. Here, however, we demonstrated that global, but not liver-specific, deletion of PKCε in mice protected against diet-induced glucose intolerance and insulin resistance. Furthermore, PKCε-dependent alterations in insulin receptor phosphorylation were not detected. Adipose-tissue-specific knockout mice did exhibit improved glucose tolerance, but phosphoproteomics revealed no PKCε-dependent effect on the activation of insulin signaling pathways. Altered phosphorylation of adipocyte proteins associated with cell junctions and endosomes was associated with changes in hepatic expression of several genes linked to glucose homeostasis and lipid metabolism. The primary effect of PKCε on glucose homeostasis is, therefore, not exerted directly in the liver as currently posited, and PKCε activation in this tissue should be interpreted with caution. However, PKCε activity in adipose tissue modulates glucose tolerance and is involved in crosstalk with the liver.

INTRODUCTION

Type 2 diabetes (T2D) is reaching epidemic proportions throughout the world (Chatterjee et al., 2017), and understanding the progression of the disease is crucial to the development of effective treatments (DeFronzo et al., 2015). Hepatic insulin resistance contributes significantly to the defective glucose homeostasis observed in T2D and has been strongly associated with obesity and fatty acid (FA) oversupply (Samuel and Shulman, 2016). Proposed mechanisms for this include the accumulation of diacylglycerol (DAG) and activation of the novel protein kinase C (PKC) isoform PKCε (Schmitz-Peiffer, 2013; Shulman, 2014). This is based on observations that whole-body PKCε knockout (KO) mice exhibited complete protection from high-fat-diet (HFD)-induced glucose intolerance, together with lower plasma insulin levels, indicating improved insulin sensitivity in the early stages of fat-diet feeding (Raddatz et al., 2011). Similarly, knockdown of PKCε *in vivo* using an antisense oligonucleotide was able to rescue the suppression of hepatic glucose production during hyperinsulinemic-euglycemic clamps in mice fed a HFD for 3 days (Samuel et al., 2007). Further studies have suggested that PKCε directly phosphorylates the insulin receptor, which reduces insulin-stimulated tyrosine kinase activity and downstream signaling, resulting in hepatic insulin resistance (Petersen et al., 2016).

However, a more complex role for PKCε emerges from other results highlighting multiple actions of the kinase. Thus, longer-term diet studies demonstrated effects on insulin secretion and insulin clearance that resulted in higher insulin levels upon glucose challenge that could compensate for insulin resistance (Schmitz-Peiffer et al., 2007), confounding our understanding of the contribution of PKCε to glucose homeostasis (Schmitz-Peiffer and Biden, 2008). Furthermore, alterations in hepatic DAG levels do not always correlate with the expected changes in insulin resistance. For example, there is controversy over whether the increased amounts of DAG observed upon overexpression of acyl-CoA:diacylglycerol acyltransferase 2 in the liver cause impaired suppression of glucose output (Jornayvaz et al., 2011; Monetti et al., 2007). Importantly, a causative role for PKCε acting directly in the liver remains to be demonstrated.

We have addressed these issues here by examining glucose tolerance and insulin sensitivity in tissue-specific PKCε KO mice. Unexpectedly, mice deficient in PKCε in the liver did not show protection against glucose intolerance or hepatic insulin resistance caused by HFD feeding. In contrast, deletion of PKCε in adipose tissue resulted in improved glucose tolerance, which was associated with alterations in adipocyte protein phosphorylation and also hepatic gene expression and triglyceride (TG) storage, indicating a role for the kinase in crosstalk between adipose tissue and the liver.

RESULTS

Global Deletion of PKCε Using Floxed PKCε Mice Recapitulates Conventional Whole-Body Deletion of PKCε in the Protection against Diet-Induced Glucose Intolerance

We generated mice with the major exon of PKCε (exon 1) flanked by LoxP sites (PKCε$^{fl/fl}$) (Figure S1A). These were first crossed with mice expressing Cre recombinase under control of the ubiquitously expressed cytomegalovirus promoter (CMV-cre) (Schwenk et al., 1995) to generate mice with a global deletion of PKCε (GEpsKO mice) (Figure S1B). Because the CMV-cre transgene is sex linked, we initially studied female mice. GEpsKO mice exhibited protection against diet-induced glucose tolerance, after both 1 and 10 weeks on an HFD (Figures 1A and 1B). Plasma insulin levels were elevated only in the longer term (Figures S1C and S1D), consistent with the time-dependent phenotypes of conventional whole-body PKCε KO mice, which are initially protected against insulin resistance and later exhibit improved β-cell function (Raddatz et al., 2011; Schmitz-Peiffer et al., 2007). GEpsKO mice underwent deletion of PKCε in germ cells as expected, facilitating the subsequent breeding of male mice independently of CMV-Cre transgene expression. These also exhibited the same time-dependent phenotypes in glucose tolerance and insulin release (Figures S1E–S1H). Collectively, these data validate the deletion of PKCε exon 1 as an approach to ablate PKCε.

Liver-Specific Deletion of PKCε Does Not Protect against Diet-Induced Glucose Intolerance

We next used mice expressing Cre recombinase under control of an albumin promoter (Alb-cre) (Chow et al., 2014) to generate liver-specific PKCε KO (LEpsKO) mice. These were deficient in PKCε in hepatocytes but exhibited normal PKCε expression in other insulin-sensitive tissues such as skeletal muscle (Figure S1I). Unexpectedly, however, after a 1 week HFD, neither male nor female LEpsKO mice displayed any improvement in glucose tolerance compared with littermate controls (whether wild-type, PKCε$^{fl/fl}$, or Alb-cre^{+} mice) (Figures 1C and S1J). Insulin excursions were unaffected (Figure S1K) and glucose tolerance was also unaltered in LEpsKO mice after 16 weeks on an HFD (Figure 1D). We next assessed insulin sensitivity directly by performing hyperinsulinemic-euglycemic clamps after a 1 week HFD. Male LEpsKO mice and PKCε$^{fl/fl}$ littermates were clamped at 8.0 ± 0.2 mmol/L glucose, and steady-state glucose levels were achieved in both groups. The glucose infusion rate required to maintain euglycemia was similar in each group (Figure 1E), confirming unaltered whole-body insulin sensitivity. Neither the glucose disposal rate (Figure 1F) nor the suppression of hepatic glucose output (Figures 1G and 1H) were different between groups. Similar results were obtained using female LEpsKO mice (Figures S1L–S1N).

Adipose-Tissue-Specific Deletion of PKCε Protects against Diet-Induced Glucose Intolerance

To test whether hepatic glucose metabolism could be modulated through PKCε-dependent crosstalk with adipose tissue, we next generated adipose-specific PKCε KO (AdEpsKO) mice by crossing PKCε$^{fl/+}$ mice with mice expressing Cre recombinase under the control of an adiponectin promoter (Adipoq-cre^{+}) (Wang et al., 2010) (Figure S2B). As described in STAR Methods, this approach also led to frequent germline deletion of PKCε in a heterozygous (PKCε$^{fl/Δ}$) or occasionally homozygous (PKCε$^{Δ/Δ}$) manner. This allowed us to examine glucose tolerance in AdEpsKO and PKCε$^{Δ/Δ}$ mice as well as Adipoq-cre^{+} and PKCε$^{fl/Δ}$ littermate controls. After a 1 week HFD, male and female AdEpsKO and PKCε$^{Δ/Δ}$ mice were similarly protected against glucose intolerance compared with controls (Figures 2A and 2B), without changes in plasma insulin profiles (Figures 2C and 2D). This phenotype was maintained in AdEpsKO mice for 16 weeks of fat feeding (Figures 2E–2H). Glucose-stimulated insulin secretion from pancreatic islets isolated from 16-week fat-fed AdEpsKO mice, and controls also did not differ (Figure S2C). In contrast, PKCε$^{Δ/Δ}$ mice were more strongly protected than AdEpsKO mice after 16 weeks, in keeping with the expected increase in insulin response of the globally deleted animals, especially in females (Figures 2G and 2H).

We next performed hyperinsulinemic-euglycemic clamps on AdEpsKO and PKCε$^{Δ/Δ}$ mice after a 1 week HFD (Figure 3A). Compared with PKCε$^{fl/Δ}$ controls, the glucose infusion rate was increased by 32% in female PKCε$^{Δ/Δ}$ mice but not significantly in AdEpsKO mice (Figure 3B). Peripheral glucose disposal was similar in all three groups (Figure 3C). In contrast, suppression of hepatic glucose production was markedly greater in PKCε$^{Δ/Δ}$ mice compared with AdEpsKO and PKCε$^{fl/Δ}$ control mice, which did not differ significantly (Figures 3D and 3E). Similar results were obtained in clamp experiments using male mice (Figures S2D–S2H).

The improvement in glucose tolerance but not hepatic insulin sensitivity of AdEpsKO mice may be explained by enhanced glucose effectiveness, which accounts for approximately 50% of glucose clearance and is modulated in part by the supply of FAs and gluconeogenic substrates from adipose tissue (Dube et al., 2015; Perry et al., 2015). We examined this using adipose tissue explants from AdEpsKO and PKCε$^{fl/Δ}$ control mice, but did not observe any differences in basal or isoproterenol-stimulated lipolysis, nor its suppression by insulin (Figure S3A); insulin-stimulated glucose uptake was also not different (Figure S3B). Furthermore, measurements of plasma free FAs during the glucose tolerance tests performed after 1 and 16 week HFD feeding (Figure 3) did not reveal differences in FA suppression (Figures S3C–S3F). Similarly, adipose tissue explants did not exhibit any PKCε-dependent differences in the release of FAs or the gluconeogenic substrates glycerol or lactate when incubated in the presence of low (5 mM) or high (25 mM) glucose, with or without insulin (Figures S3G–S3I), while alanine release was not detected. In addition, fat-fed AdEpsKO mice did not exhibit alterations in total body weight or fat mass, similar to our findings of GEpsKO and LEpsKO mice (Figures S3J and S3K) and also conventional whole-body PKCε KO mice (Raddatz et al., 2011).

Effects of PKCε Deletion on Hepatic Insulin Receptor Phosphorylation and on the Adipocyte Phosphoproteome

PKCε has been proposed to directly phosphorylate the insulin receptor at a threonine residue in the tyrosine kinase activation loop in liver to inhibit insulin signaling (referred to as Thr1160; Petersen et al., 2016). We therefore used liquid chromatography-tandem

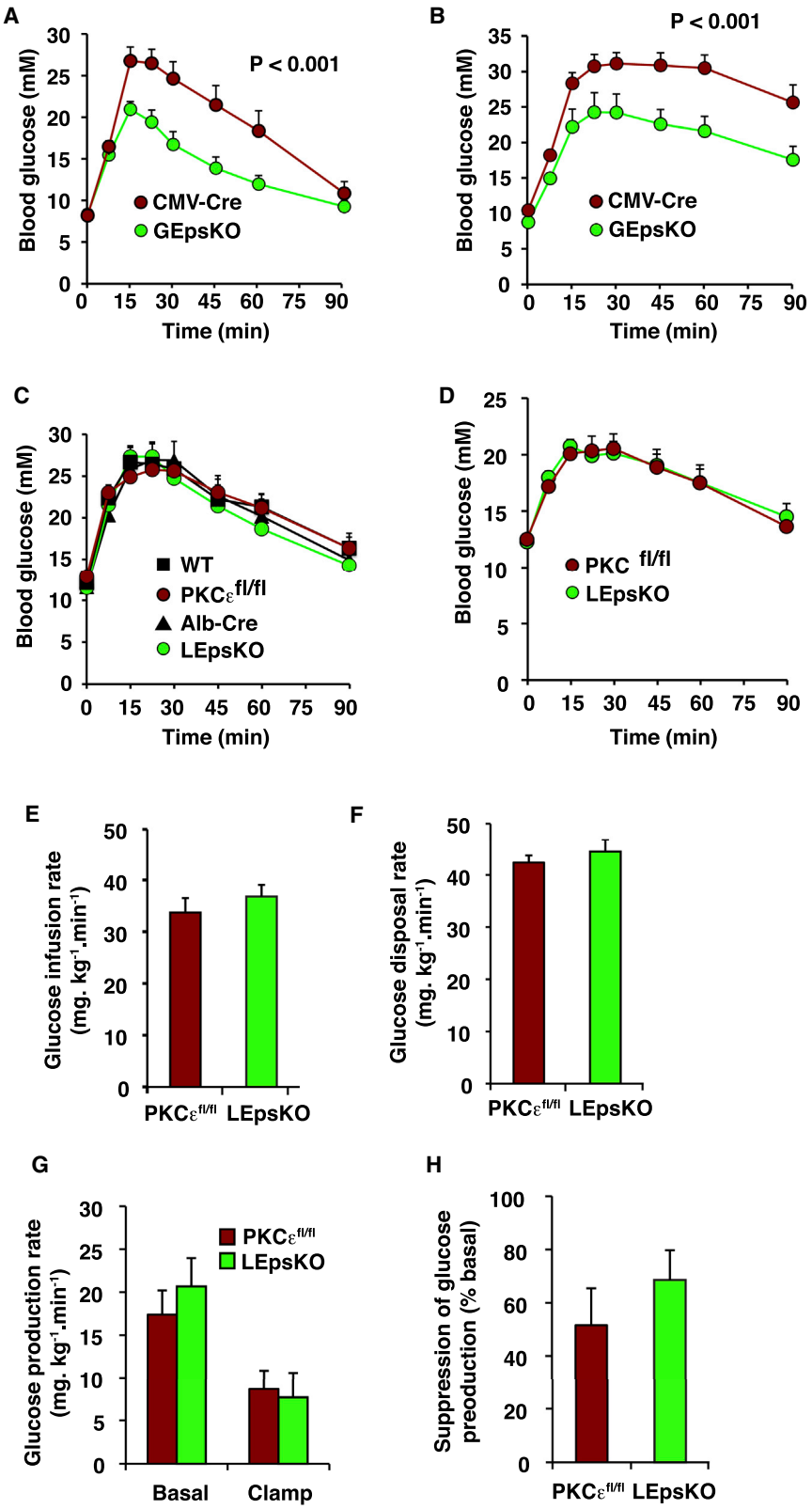

Figure 1. Global, but Not Hepatocyte-Specific, Deletion of PKCε Protects against Diet-Induced Glucose Intolerance

For a Figure360 author presentation of Figure 1, see https//dx.doi:10.1016/j.cmet.2018.09.013#mmc4. Figure360▷

(A and B) Female GEpsKO and CMV-Cre control mice were fed an HFD for 10 weeks and subjected to intraperitoneal glucose tolerance tests (2 g/kg) at 1 and 10 weeks (n = 9 control, n = 7 GEpsKO).

(A) Glucose tolerance test in GEpsKO mice and littermate controls fed an HFD for 1 week. ANOVA, $p < 0.001$, main effect for PKCε deletion.

(B) Glucose tolerance test in GEpsKO mice and littermate controls fed an HFD for 10 weeks. ANOVA, $p < 0.001$, main effect for PKCε deletion.

(C–H) Male LEpsKO mice and littermate controls (Alb-Cre, $PKC\varepsilon^{fl/fl}$ and WT mice) were fed an HFD for up to 16 weeks and subjected to intraperitoneal glucose tolerance tests and hyperinsulinemic-euglycemic clamping.

(C) Glucose tolerance test (2 g/kg) in male LEpsKO mice and littermate controls fed an HFD for 1 week (n = 9 LEpsKO, n = 14 $PKC\varepsilon^{fl/fl}$, n = 4 Alb-Cre, n = 5 WT).

(D) Glucose tolerance test (0.5 g/kg) in male LEpsKO mice (n = 13) and littermate controls ($PKC\varepsilon^{fl/fl}$ mice, n = 10) fed an HFD for 16 weeks.

(E) Glucose infusion rate during clamping after a 1 week HFD (n = 8 per group).

(F) Insulin-stimulated whole-body glucose disposal rate.

(G) Basal and insulin-stimulated rates of glucose production.

(H) Suppression of hepatic glucose output by insulin.

All data are represented as means ± SEM.

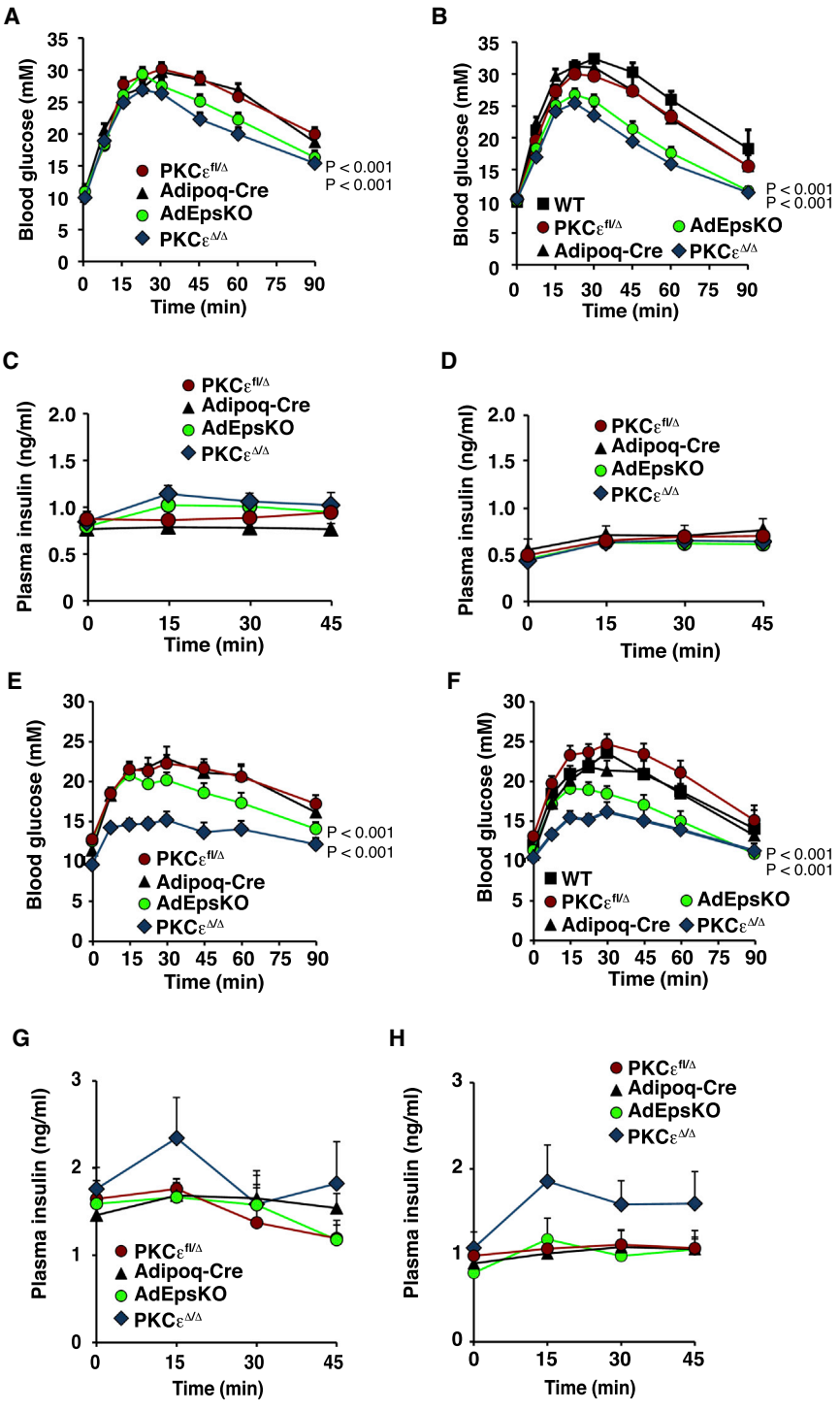

Figure 2. Deletion of PKCε in Adipose Tissue Recapitulates Effects of Global Deletion on Glucose Tolerance in Fat-Fed Mice

(A–H) Male and female AdEpsKO, PKCε$^{\Delta/\Delta}$, and littermate control mice were fed an HFD for 16 weeks and subjected to intraperitoneal glucose tolerance tests (2 g/kg at 1 week; 0.5 g/kg at 16 weeks) (males n = 12 AdEpsKO, n = 5 PKCε$^{\Delta/\Delta}$, n = 17 PKCε$^{fl/\Delta}$, n = 13 adipoq-cre^{+}; females n = 8 AdEpsKO, n = 10 PKCε$^{\Delta/\Delta}$, n = 17 PKCε$^{fl/\Delta}$, n = 7 adipoq-cre, n = 4 WT).

(A) Glucose tolerance test (2 g/kg) in male AdEpsKO mice and littermate controls fed an HFD for 1 week. ANOVA, $p < 0.001$, main effect for PKCε deletion in adipose tissue or whole body.

(B) Glucose tolerance test (2 g/kg) in female AdEpsKO mice and littermate controls fed an HFD for 1 week. ANOVA, $p < 0.001$, main effect for PKCε deletion in adipose tissue or whole body.

(C) Plasma insulin levels during the glucose tolerance test performed on male mice after 1 week HFD shown in (A).

(D) Plasma insulin levels during the glucose tolerance test performed on female mice after 1 week HFD shown in (B).

(E) Glucose tolerance test (0.5 g/kg) in male AdEpsKO mice and littermate controls fed an HFD for 16 weeks. ANOVA, $p < 0.001$, main effect for PKCε deletion in adipose tissue or whole body.

(F) Glucose tolerance test (0.5 g/kg) in female AdEpsKO mice and littermate controls fed an HFD for 16 weeks. ANOVA, $p < 0.001$, main effect for PKCε deletion in adipose tissue or whole body.

(G) Plasma insulin levels during the glucose tolerance test performed on male mice after 16 weeks HFD shown in (E).

(H) Plasma insulin levels during the glucose tolerance test performed on female mice after 16 weeks HFD shown in (F). ANOVA: $p < 0.005$, main effect for whole-body PKCε deletion.

All data are represented as means ± SEM.

mass spectrometry (LC-MS/MS) to determine whether this was affected by global PKCε deficiency. Following immunoprecipitation of the receptor from extracts of fat-fed GEpsKO and CMV-cre mouse livers, we observed phosphorylation of Tyr-1175 and Tyr-1179 (mouse sequence) in the peptide derived from the activation loop as expected (Figure S4A; Table S1). However, phosphorylation of Thr-1177, corresponding to the site phosphorylated *in vitro* by PKCε (Petersen et al., 2016) was not detected. Furthermore, in our hands, PKCε *in vitro* kinase activity promoted phosphorylation of Ser-1340 of the immunoprecipitated insulin receptor but not Thr-1177 (Figure S4B; Table S1). The physiological importance of Ser-1340 phosphorylation is unclear, especially since Ser-1340 is not conserved in the human protein. These data provide further evidence against the hypothesis that PKCε generates insulin resistance directly in the liver by phosphorylation of the insulin receptor.

We extended our proteomic approach to adipose tissue, where PKCε deletion had the greatest effect on glucose tolerance. Only limited changes were observed in protein abundance when comparing tissue from fat-fed AdEpsKO and control mice (Figure S4C). Similarly, RNA sequencing (RNA-seq) showed differential expression of a relatively small number of genes (Figure S4D). We next interrogated the PKCε-dependent phosphoproteome. Primary adipocytes isolated from AdEpsKO and

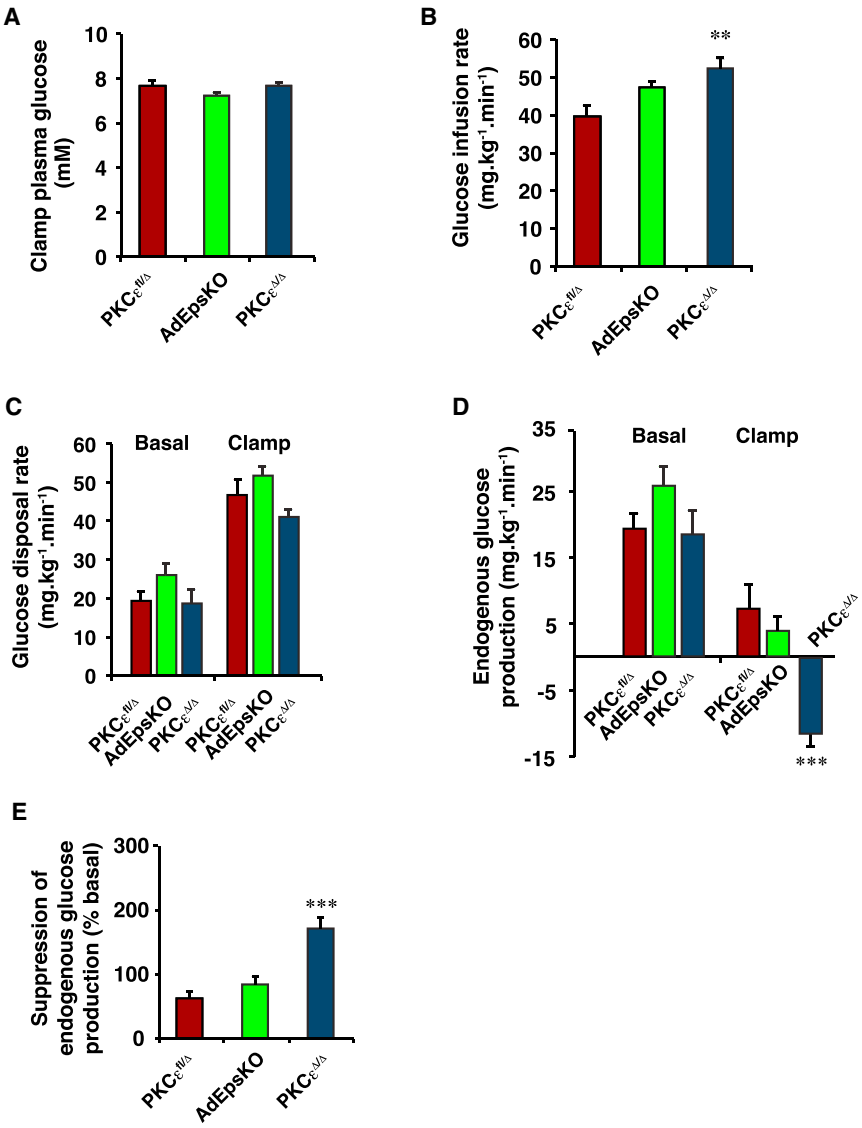

Figure 3. Whole-Body, but Not Adipose-Tissue-Specific, Deletion of PKCε Improves Insulin Sensitivity in Fat-Fed Mice

Female PKCε$^{fl/\Delta}$, AdEpsKO, and PKCε$^{\Delta/\Delta}$ mice were subjected to hyperinsulinemic-euglycemic clamping after a 1 week HFD (n = 8 PKCε$^{fl/\Delta}$, n = 6 AdEpsKO, n = 5 PKCε$^{\Delta/\Delta}$).

(A) Blood glucose levels during clamping.

(B) Glucose infusion rate during clamping. t test **p < 0.02 versus PKCε$^{fl/\Delta}$.

(C) Basal and insulin-stimulated whole-body glucose disposal rates.

(D) Basal and insulin-stimulated rates of glucose production. t test ***p < 0.001 versus PKCε$^{fl/\Delta}$.

(E) Suppression of glucose output by insulin. t test ***p < 0.001 versus PKCε$^{fl/\Delta}$.

All data are represented as means ± SEM.

PKCε$^{fl/\Delta}$ mice were stimulated with insulin and glucose to mimic the conditions under which improved glucose tolerance was most evident in AdEpsKO mice. A total of 302 phosphorylation sites were significantly regulated in PKCε$^{fl/\Delta}$ control cells subject to insulin stimulation relative to basal conditions (false discovery rate [FDR] < 0.1) (Table S2), including components of the canonical INSR/IRS/AKT/mTOR signaling pathways (Figures 4A and 4B). Phosphorylation of these was not significantly different in cells from AdEpsKO mice, which was confirmed by immunoblotting (Figure 4C). In contrast, the phosphorylation of 559 sites in other proteins significantly decreased in PKCε-deficient cells (Figure 4D). These proteins were enriched for association with either the endosome, nuclear compartments, or cell junctions, especially focal adhesions and adherens junctions, and also for pathways regulating small monomeric G-proteins (Figure 4E; Table S2). Consistent with a remodeling of adipose tissue, histological analysis of tissue from long-term fat-fed mice indicated a redistribution of adipocyte size toward smaller cells in the absence of PKCε (Figure 4F), despite the unaltered fat mass.

These PKCε-dependent changes in adipose tissue may reflect alterations in its endocrine function, and we therefore examined whether they were associated with indirect effects on the liver. A 1 week HFD caused a significant increase in TG accumulation in livers from AdEpsKO mice (Figures S4E and S4H), again similar to whole-body PKCε KO mice (Raddatz et al., 2011). There were no accompanying changes in liver DAG or ceramide levels (Figures S4F, S4G, S4I, and S4J), and only minor changes were observed in other specific lipid species (Figure S4K). RNA-seq indicated that in marked contrast to adipose tissue, 146 genes were differentially regulated in the liver of AdEpsKO mice (Figures S4L and S4M). Gene set enrichment analysis indicated that PKCε deletion in adipose tissue affected the hepatic expression of genes involved in liver development, iron and erythrocyte homeostasis, fatty liver, and steatohepatitis (Figures S4N and S4O). Thus, alterations in the adipocyte phosphoproteome are associated with hepatic TG storage and gene expression, indicative of PKCε-dependent crosstalk between adipose tissue and the liver.

DISCUSSION

The key finding of our current study is that the inhibitory effects of PKCε action on whole-body glucose tolerance and insulin sensitivity are not exerted directly in the liver as previously thought (Samuel et al., 2007). Instead, we demonstrate that deletion of the kinase specifically in adipose tissue accounts predominantly for the protection against diet-induced glucose intolerance observed in whole-body PKCε KO mice. This challenges the notion that PKCε activation in hepatocytes is an important driver of insulin resistance.

By making comparisons between different lines of PKCε-deficient mice, all derived from our PKCε$^{fl/fl}$ mice, we are able to

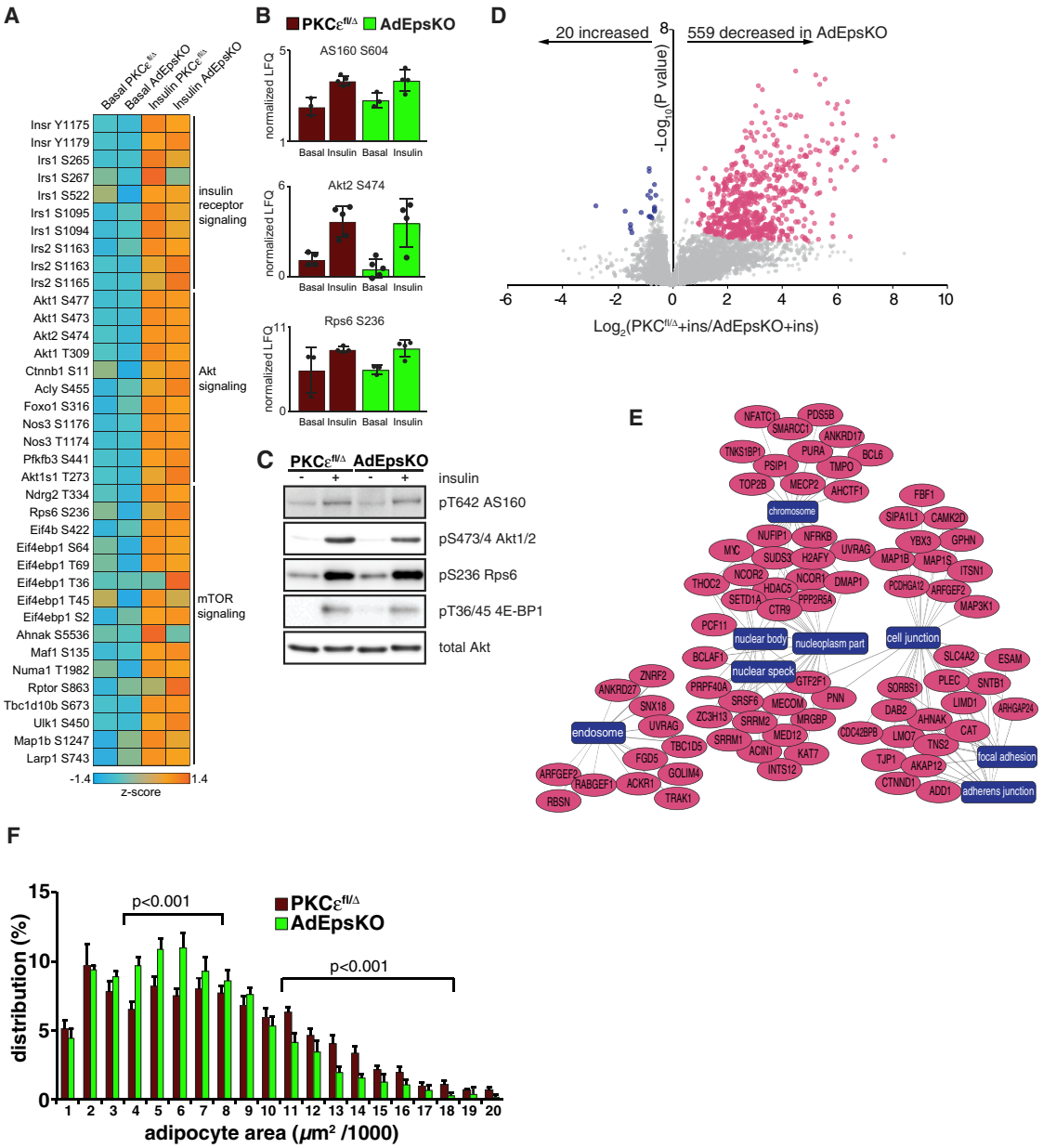

Figure 4. Adipocytes from AdEpsKO Mice Exhibit Alterations in the Phosphorylation of Proteins Linked to Cell Adhesion, but Not Insulin Signaling

(A–E) Adipocytes harvested from AdEpsKO and PKCε$^{fl/\Delta}$ mice were incubated in the presence or absence of insulin and high glucose, and proteins subjected to phosphoproteomic analysis by mass spectrometry (n = 4, AdEpsKO; n = 5, PKCε$^{fl/\Delta}$).

(A) Heatmap illustrating the lack of effect of PKCε deletion on the phosphorylation of insulin signaling proteins in adipocytes incubated under basal conditions or stimulated with insulin in the presence of high glucose. Sites indicated refer to mouse sequences; phosphorylation levels are expressed as *Z* scores for ease of comparison.

(B) Histograms indicating phosphorylation of insulin signaling components in adipocytes under the conditions indicated, determined by mass spectrometry. All data are represented as means ± SEM.

(C) Phosphorylation of insulin signaling components in adipocytes from AdEpsKO and PKCε$^{fl/\Delta}$ mice under the conditions indicated, determined by immunoblotting.

(D) Volcano plot of adipocyte proteins differentially phosphorylated by PKCε deletion in the presence of insulin and glucose (FDR <0.1).

(E) Network generated using Cytoscape, indicating the enrichment of differentially phosphorylated proteins (ellipses) according to cellular compartment (rectangles).

(F) Distribution of adipocyte size in adipose tissue from fat-fed AdEpsKO and PKCε$^{fl/\Delta}$ mice, determined by analysis of images from H&E-stained sections (n = 7, AdEpsKO; n = 7, PKCε$^{fl/\Delta}$). ANOVA: $p < 0.005$, main effect for adipose PKCε deletion over the indicated size ranges. All data are represented as means ± SEM.

exclude several trivial explanations for our unexpected findings. Firstly, the absence of a metabolic phenotype in LEpsKO mice cannot be explained by a failure of our deletion strategy targeting PKCε exon 1, because this did produce the expected phenotypes in GEpsKO mice as well as improved glucose tolerance in AdEpsKO mice. Nor can the phenotype of AdEpsKO mice be explained by an impact on liver due to an undetected germline PKCε deletion (Lee et al., 2013), because in that case insulin secretion would also have been increased in the longer term, as consistently observed upon global deletion (Schmitz-Peiffer et al., 2007 and Figures 2 and S1). Secondly, the phenotypes observed upon global deletion, together with the absence of changes in the expression of other PKC isoforms in liver (Raddatz et al., 2011), argue against the occurrence of any compensatory mechanisms in LEpsKO mice. Thirdly, the marked improvement in the suppression of hepatic glucose output exhibited by fat-fed PKCε$^{\Delta/\Delta}$ mice also demonstrates that the hyperinsulinemic-euglycemic clamps were sufficiently sensitive to detect a hepatocyte-autonomous effect of PKCε deletion, if one existed.

PKCε depletion *in vivo* using an antisense oligonucleotide also resulted in improved hepatic insulin sensitivity that was ascribed to direct effects on insulin signaling in liver (Samuel et al., 2007). In the light of our results, this is more likely to be explained by a loss of PKCε in other tissues. Indeed, knockdown in adipose tissue was also reported but not considered a contributing factor (Samuel et al., 2007). The metabolic findings of this previous study are, therefore, not in disagreement with the data presented here but need to be reinterpreted. Likewise, almost 50 subsequent studies, by the Shulman group and others, equate the association between PKCε activation and insulin resistance with a causative mechanism and need to be re-evaluated.

Our current findings also argue against the hypothesis that PKCε directly mediates inhibitory insulin receptor phosphorylation (Petersen et al., 2016). We presented evidence that PKCε phosphorylates Ser-1340 *in vitro*, but probably not *in vivo*, and this site is not conserved in humans. Peterson et al. previously reported Thr-1160 phosphorylation (Thr 1177 in the mouse receptor) by PKCε *in vitro*. Key criteria that confirm the physiological relevance of an *in vitro* phosphorylation event include demonstrations that (1) it occurs in intact cells in response to stimuli that are known to activate the kinase, (2) it is prevented by drugs that inhibit the kinase, and (3) it does not occur in KO mice lacking the kinase (Cohen and Knebel, 2006). These were not addressed (Petersen et al., 2016), and it is possible that phosphorylation of Thr-1177 is mediated by another kinase *in vivo*. Our results are consistent with our previous data, showing firstly that upon short-term fat feeding, whole-body PKCε deletion restores glucose tolerance in the absence of any defect in hepatic insulin signaling (Raddatz et al., 2011), and secondly that upon long-term fat feeding, when signaling is perturbed, PKCε deletion does not restore insulin receptor, IRS-1, or Akt phosphorylation (Schmitz-Peiffer et al., 2007). Other studies have also shown that initially, fat-diet-induced insulin resistance is independent of signaling defects (Hoehn et al., 2008; Turner et al., 2013).

Our data, therefore, imply that even if PKCε activation occurs in response to fat-diet-induced DAG accumulation in the liver, it does not play a major role in whole-body glucose intolerance or hepatic insulin resistance. PKCε has also, however, been implicated in adipocyte differentiation and metabolism (Fleming et al., 1998; Nakamura, 2010; Webb et al., 2003), and conversely, changes in adipose tissue PKCε expression and activation have been linked to obesity and glucose intolerance (Frevert and Kahn, 1996; Qu et al., 1999). Our current studies now suggest that PKCε may mediate crosstalk between adipose tissue and liver. Thus, we showed that loss of PKCε in adipose tissue impacted more strongly on gene expression profiles in liver than it did in adipose tissue itself. In addition, AdEpsKO mice displayed a small but significant increase in liver TG storage. This was also seen in conventional whole-body KO mice (Schmitz-Peiffer et al., 2007) and might reflect beneficial alterations in hepatic substrate fluxes resulting in enhanced glucose effectiveness. However, we did not observe any changes in mobilization of gluconeogenic substrates or FAs from adipose explants that might account for the improved glucose tolerance. Indeed, although whole-body PKCε deletion reduces FA availability to the liver upon starvation for ketogenesis (Raddatz et al., 2012), AdEpsKO mice do not exhibit this phenotype (data not shown). It seems likely, therefore, that the functional crosstalk that we have observed is mediated by the PKCε-dependent release of secretory factors into the circulation. This may be linked to the increased prevalence of smaller cells in the AdEpsKO mice, which is consistent with beneficial changes in adipose tissue function, including the secretion of factors affecting glucose and lipid metabolism in other tissues (Tandon et al., 2018). The identification of PKCε-dependent phosphorylation of proteins associated with endosomes, GEF, and GAP activity is also in agreement with such changes. The precise mechanisms linking the direct action of PKCε in adipose tissue to the modulation of hepatic metabolism remain to be determined and are probably complex. Other sites of PKCε action must also contribute to the overall phenotype, indicated by the improvement in liver insulin sensitivity observed in global PKCε-deficient (PKCε$^{\Delta/\Delta}$) mice but not AdEpsKO mice.

Altogether, this study has enabled us to make major discoveries that redefine the role of PKCε in glucose homeostasis. Firstly, we unexpectedly showed that ablation of PKCε solely in hepatocytes is not sufficient to protect mice against diet-induced glucose intolerance or insulin resistance. Secondly, we demonstrated that deletion of the kinase in adipose tissue can improve glucose tolerance, although this does not appear to be linked to the suppression of glucose production. Thirdly, we have identified the PKCε-dependent phosphoproteome in adipocytes, implicating roles for cell-cell contact and endosome function. We provide evidence for significant PKCε-dependent crosstalk between adipose tissue and the liver that results in the modulation of several diabetes- and steatosis-related genes as well as those of TG storage. The new insights provided here will guide future studies to determine the direct effects of PKCε and the communication it drives between adipose tissue and the liver.

Limitations of the Study

Ideally, mice without heterozygous global PKCε deletion would have been used for the study of PKCε action in adipose tissue, but this was not feasible due to the low frequency of

Adipoq-$^{cre/+}$/PKCε$^{fl/fl}$ mice. Our studies are appropriately controlled because both AdEpsKO and control PKCε$^{fl/\Delta}$ mice harbored the heterozygous global deletion. Importantly, while our findings may underestimate the beneficial effects of PKCε deletion in adipose tissue, due to this background, they were not compromised by any insulin secretory phenotype in AdEpsKO mice (Figures 2C, 2D, 2G, 2H, and S2C). We were also unable to identify the direct site of PKCε action that explains the improvement in hepatic insulin sensitivity observed in PKCε$^{\Delta/\Delta}$ mice (Figures 3D and 3E), which will require deletion of the kinase in further tissues. Finally, the nature of the PKCε-dependent crosstalk between adipose tissue and the liver remains to be determined.

A recent study employed antisense oligonucleotides to examine the effects of PKCε knockdown on the phosphoproteome in rat liver, highlighting PKCε interactions with insulin signaling (Gassaway et al., 2018). The oligonucleotides employed also knock down PKCε in adipose tissue (Samuel et al., 2007), and as discussed above, our data suggest that their beneficial effects on whole-body glucose homeostasis are more likely mediated through adipose tissue and not at the level of insulin signal transduction.

STAR★METHODS

Detailed methods are provided in the online version of this paper and include the following:

- KEY RESOURCES TABLE
- CONTACT FOR REAGENT AND RESOURCE SHARING
- EXPERIMENTAL MODEL AND SUBJECT DETAILS
  - Mouse Models
- METHOD DETAILS
  - Mouse Diet Feeding
  - Intraperitoneal Glucose Tolerance Test (ipGTT)
  - Hyperinsulinemic-Euglycemic Clamps
  - Immunoblotting
  - Release of Free Fatty Acids and Gluconeogenic Substrates from Adipose Tissue Explants
  - Glucose Transport in Adipose Tissue Explants
  - Lipid Analysis
  - RNA-Seq Analysis
  - Insulin Receptor Immunoprecipitation, In-gel Protein Digestion and Peptide Extraction
  - Primary Adipocyte Isolation, Incubation and Protein Preparation for Proteomic and Phosphoproteomic Analyses
  - Phosphopeptide Enrichment
  - Mass Spectrometry
  - Analysis of Mass Spectrometry Data
  - Histology and Adipocyte Size Measurement
  - Quantitative Real-Time-PCR (qRT-PCR)
- QUANTIFICATION AND STATISTICAL ANALYSIS
- DATA AND SOFTWARE AVAILABILITY

SUPPLEMENTAL INFORMATION

Supplemental Information includes four figures and two tables and can be found with this article online at https://doi.org/10.1016/j.cmet.2018.09.013.

ACKNOWLEDGMENTS

The authors wish to acknowledge the expert technical assistance of the Garvan Institute Biological Testing Facility and Dr. Emma Estevez. We also thank Natalie Mellett for lipidomic technical assistance. M.A.F. (APP1116936) and D.E.J. (APP1117078) are supported by fellowships from the NHMRC of Australia. This project was supported by project grants from the NHMRC of Australia (APP1081869, 535917) and Diabetes Australia Research Trust (Y15G-SCHC, Y06G-SCHC) to C.S.-P.

AUTHOR CONTRIBUTIONS

A.E.B., B.M.L., B.D., K.R., S.A.M., L.O., D.H., and C.S.-P. conducted *in vivo* and *ex vivo* mouse studies. B.M.L., E.K., and A.G.v.d.K. carried out qRT-PCR analyses. B.L.P. performed total and phosphoproteomic analyses. D.C.H. and P.J.M. conducted lipidomic analyses. S.R. performed RNA-seq and bioinformatic analyses. G.J.C., D.E.J., and M.A.F. provided supervision and guidance for clamp studies, proteomics, and bioinformatic analyses. T.J.B. and C.S.-P. conceived experiments and provided supervision, guidance, and funding; C.S.-P. directed the project, analyzed the data, and wrote the manuscript. All the authors discussed the results and commented on the manuscript.

DECLARATION OF INTERESTS

T.J.B. and C.S.-P. are named inventors on US patent 8,598,146 concerning modulators of protein kinase C epsilon.

Received: February 1, 2018
Revised: July 16, 2018
Accepted: September 12, 2018
Published: October 11, 2018

REFERENCES

Ayala, J.E., Bracy, D.P., McGuinness, O.P., and Wasserman, D.H. (2006). Considerations in the design of hyperinsulinemic-euglycemic clamps in the conscious mouse. Diabetes *55*, 390–397.

Benjamini, Y., and Hochberg, Y. (1995). Controlling the false discovery rate: a practical and powerful approach to multiple testing. J. R. Stat. Soc. Ser. B Stat. Methodol. *57*, 289–300.

Brandon, A.E., Stuart, E., Leslie, S.J., Hoehn, K.L., James, D.E., Kraegen, E.W., Turner, N., and Cooney, G.J. (2016). Minimal impact of age and housing temperature on the metabolic phenotype of Acc2-/- mice. J. Endocrinol. *228*, 127–134.

Burchfield, J.G., Lennard, A.J., Narasimhan, S., Hughes, W.E., Wasinger, V.C., Corthals, G.L., Okuda, T., Kondoh, H., Biden, T.J., and Schmitz-Peiffer, C. (2004). Akt mediates insulin-stimulated phosphorylation of Ndrg2: evidence for cross-talk with protein kinase C theta. J. Biol. Chem. *279*, 18623–18632.

Chatterjee, S., Khunti, K., and Davies, M.J. (2017). Type 2 diabetes. Lancet *389*, 2239–2251.

Chow, J.D., Lawrence, R.T., Healy, M.E., Dominy, J.E., Liao, J.A., Breen, D.S., Byrne, F.L., Kenwood, B.M., Lackner, C., Okutsu, S., et al. (2014). Genetic inhibition of hepatic acetyl-CoA carboxylase activity increases liver fat and alters global protein acetylation. Mol. Metab. *3*, 419–431.

Cohen, P., and Knebel, A. (2006). KESTREL: a powerful method for identifying the physiological substrates of protein kinases. Biochem. J. *393*, 1–6.

Cox, J., and Mann, M. (2008). MaxQuant enables high peptide identification rates, individualized p.p.b.-range mass accuracies and proteome-wide protein quantification. Nat. Biotechnol. *26*, 1367–1372.

DeFronzo, R.A., Ferrannini, E., Groop, L., Henry, R.R., Herman, W.H., Holst, J.J., Hu, F.B., Kahn, C.R., Raz, I., Shulman, G.I., et al. (2015). Type 2 diabetes mellitus. Nat. Rev. Dis. Primers *1*, 15019.

Dobin, A., Davis, C.A., Schlesinger, F., Drenkow, J., Zaleski, C., Jha, S., Batut, P., Chaisson, M., and Gingeras, T.R. (2013). STAR: ultrafast universal RNA-seq aligner. Bioinformatics *29*, 15–21.

Dube, S., Errazuriz-Cruzat, I., Basu, A., and Basu, R. (2015). The forgotten role of glucose effectiveness in the regulation of glucose tolerance. Curr. Diab. Rep. *15*, 605.

Fleming, I., Mackenzie, S.J., Vernon, R.G., Anderson, N.G., Houslay, M.D., and Kilgour, E. (1998). Protein kinase c isoforms play differential roles in the regulation of adipocyte differentiation. Biochem. J. *333*, 719–727.

Frevert, E.U., and Kahn, B.B. (1996). Protein kinase C isoforms epsilon, eta, delta and zeta in murine adipocytes: expression, subcellular localization and tissue-specific regulation in insulin-resistant states. Biochem. J. *316*, 865–871.

Gassaway, B.M., Petersen, M.C., Surovtseva, Y.V., Barber, K.W., Sheetz, J.B., Aerni, H.R., Merkel, J.S., Samuel, V.T., Shulman, G.I., and Rinehart, J. (2018). PKCε contributes to lipid-induced insulin resistance through cross talk with p70S6K and through previously unknown regulators of insulin signaling. Proc. Natl. Acad. Sci. U S A. https://doi.org/10.1073/pnas.1804379115.

Gutmann, I., and Wahlefeld, A.W., eds. (1974). l-(+)-Lactate Determination with Lactate Dehydrogenase and NAD, *vol. 3* (Academic Press), pp. 1464–1468.

Hoehn, K.L., Hohnen-Behrens, C., Cederberg, A., Wu, L.E., Turner, N., Yuasa, T., Ebina, Y., and James, D.E. (2008). IRS1-independent defects define major nodes of insulin resistance. Cell Metab. *7*, 421–433.

Honnor, R.C., Dhillon, G.S., and Londos, C. (1985). cAMP-dependent protein kinase and lipolysis in rat adipocytes. I. Cell preparation, manipulation, and predictability in behavior. J. Biol. Chem. *260*, 15122–15129.

Huang da, W., Sherman, B.T., and Lempicki, R.A. (2009). Systematic and integrative analysis of large gene lists using DAVID bioinformatics resources. Nat. Protoc. *4*, 44–57.

Humphrey, S.J., Azimifar, S.B., and Mann, M. (2015). High-throughput phosphoproteomics reveals in vivo insulin signaling dynamics. Nat. Biotechnol. *33*, 990–995.

Jornayvaz, F.R., Birkenfeld, A.L., Jurczak, M.J., Kanda, S., Guigni, B.A., Jiang, D.C., Zhang, D., Lee, H.Y., Samuel, V.T., and Shulman, G.I. (2011). Hepatic insulin resistance in mice with hepatic overexpression of diacylglycerol acyltransferase 2. Proc. Natl. Acad. Sci. U S A *108*, 5748–5752.

Kaimal, V., Bardes, E.E., Tabar, S.C., Jegga, A.G., and Aronow, B.J. (2010). ToppCluster: a multiple gene list feature analyzer for comparative enrichment clustering and network-based dissection of biological systems. Nucleic Acids Res. *38*, W96–W102.

Lee, K.Y., Russell, S.J., Ussar, S., Boucher, J., Vernochet, C., Mori, M.A., Smyth, G., Rourk, M., Cederquist, C., Rosen, E.D., et al. (2013). Lessons on conditional gene targeting in mouse adipose tissue. Diabetes *62*, 864–874.

Li, B., and Dewey, C.N. (2011). RSEM: accurate transcript quantification from RNA-seq data with or without a reference genome. BMC Bioinformatics *12*, 323.

Love, M.I., Huber, W., and Anders, S. (2014). Moderated estimation of fold change and dispersion for RNA-seq data with DESeq2. Genome Biol. *15*, 550.

Monetti, M., Levin, M.C., Watt, M.J., Sajan, M.P., Marmor, S., Hubbard, B.K., Stevens, R.D., Bain, J.R., Newgard, C.B., Farese, R.V., Sr., et al. (2007). Dissociation of hepatic steatosis and insulin resistance in mice overexpressing DGAT in the liver. Cell Metab. *6*, 69–78.

Nakamura, J. (2010). Phorbol 12-myristate 13-acetate inhibits the antilipolytic action of insulin, probably via the activity of protein kinase Cε. Eur. J. Pharmacol. *648*, 188–194.

Perry, R.J., Camporez, J.P., Kursawe, R., Titchenell, P.M., Zhang, D., Perry, C.J., Jurczak, M.J., Abudukadier, A., Han, M.S., Zhang, X.M., et al. (2015). Hepatic acetyl CoA links adipose tissue inflammation to hepatic insulin resistance and type 2 diabetes. Cell *160*, 745–758.

Petersen, M.C., Madiraju, A.K., Gassaway, B.M., Marcel, M., Nasiri, A.R., Butrico, G., Marcucci, M.J., Zhang, D., Abulizi, A., Zhang, X.M., et al. (2016). Insulin receptor Thr1160 phosphorylation mediates lipid-induced hepatic insulin resistance. J. Clin. Invest. *126*, 4361–4371.

Qu, X.Q., Seale, J.P., and Donnelly, R. (1999). Tissue- and isoform-specific effects of aging in rats on protein kinase C in insulin-sensitive tissues. Clin. Sci. *97*, 355–361.

Raddatz, K., Frangioudakis, G., Diakanastasis, B., Liao, B.M., Leitges, M., and Schmitz-Peiffer, C. (2012). Deletion of protein kinase Cε in mice has limited effects on liver metabolite levels but alters fasting ketogenesis and gluconeogenesis. Diabetologia *55*, 2789–2793.

Raddatz, K., Turner, N., Frangioudakis, G., Liao, B.M., Pedersen, D.J., Cantley, J., Wilks, D., Preston, E., Hegarty, B.D., Leitges, M., et al. (2011). Time-dependent effects of Prkce deletion on glucose homeostasis and hepatic lipid metabolism on dietary lipid oversupply in mice. Diabetologia *54*, 1447–1456.

Rodbell, M. (1964). Metabolism of isolated fat cells. I. Effects of hormones on glucose metabolism and lipolysis. J. Biol. Chem. *239*, 375–380.

Samuel, V.T., Liu, Z.X., Wang, A., Beddow, S.A., Geisler, J.G., Kahn, M., Zhang, X.M., Monia, B.P., Bhanot, S., and Shulman, G.I. (2007). Inhibition of protein kinase Cε prevents hepatic insulin resistance in nonalcoholic fatty liver disease. J. Clin. Invest. *117*, 739–745.

Samuel, V.T., and Shulman, G.I. (2016). The pathogenesis of insulin resistance: integrating signaling pathways and substrate flux. J. Clin. Invest. *126*, 12–22.

Schilling, B., Rardin, M.J., MacLean, B.X., Zawadzka, A.M., Frewen, B.E., Cusack, M.P., Sorensen, D.J., Bereman, M.S., Jing, E., Wu, C.C., et al. (2012). Platform-independent and label-free quantitation of proteomic data using MS1 extracted ion chromatograms in skyline: application to protein acetylation and phosphorylation. Mol. Cell. Proteomics *11*, 202–214.

Schmitz-Peiffer, C. (2013). The tail wagging the dog - regulation of lipid metabolism by protein kinase C. FEBS J. *280*, 5371–5383.

Schmitz-Peiffer, C., and Biden, T.J. (2008). Protein kinase C function in muscle, liver, and beta-cells and its therapeutic implications for type 2 diabetes. Diabetes *57*, 1774–1783.

Schmitz-Peiffer, C., Laybutt, D.R., Burchfield, J.G., Gurisik, E., Narasimhan, S., Mitchell, C.J., Pedersen, D.J., Braun, U., Cooney, G.J., Leitges, M., et al. (2007). Inhibition of PKCε improves glucose-stimulated insulin secretion and reduces insulin clearance. Cell Metab. *6*, 320–328.

Schwenk, F., Baron, U., and Rajewsky, K. (1995). A cre-transgenic mouse strain for the ubiquitous deletion of loxP-flanked gene segments including deletion in germ cells. Nucleic Acids Res. *23*, 5080–5081.

Shannon, P., Markiel, A., Ozier, O., Baliga, N.S., Wang, J.T., Ramage, D., Amin, N., Schwikowski, B., and Ideker, T. (2003). Cytoscape: a software environment for integrated models of biomolecular interaction networks. Genome Res. *13*, 2498–2504.

Shulman, G.I. (2014). Ectopic fat in insulin resistance, dyslipidemia, and cardiometabolic disease. N. Engl. J. Med. *371*, 1131–1141.

Tandon, P., Wafer, R., and Minchin, J.E.N. (2018). Adipose morphology and metabolic disease. J. Exp. Biol. *221*, https://doi.org/10.1242/jeb.164970.

Turner, N., Kowalski, G.M., Leslie, S.J., Risis, S., Yang, C., Lee-Young, R.S., Babb, J.R., Meikle, P.J., Lancaster, G.I., Henstridge, D.C., et al. (2013). Distinct patterns of tissue-specific lipid accumulation during the induction of insulin resistance in mice by high-fat feeding. Diabetologia *56*, 1638–1648.

Tyanova, S., Temu, T., Sinitcyn, P., Carlson, A., Hein, M.Y., Geiger, T., Mann, M., and Cox, J. (2016). The Perseus computational platform for comprehensive analysis of (prote)omics data. Nat. Methods *13*, 731–740.

Wang, Z.V., Deng, Y., Wang, Q.A., Sun, K., and Scherer, P.E. (2010). Identification and characterization of a promoter cassette conferring adipocyte-specific gene expression. Endocrinology *151*, 2933–2939.

Webb, P.R., Doyle, C., and Anderson, N.G. (2003). Protein kinase C-epsilon promotes adipogenic commitment and is essential for terminal differentiation of 3T3-F442A preadipocytes. Cell. Mol. Life Sci. *60*, 1504–1512.

Weir, J.M., Wong, G., Barlow, C.K., Greeve, M.A., Kowalczyk, A., Almasy, L., Comuzzie, A.G., Mahaney, M.C., Jowett, J.B., Shaw, J., et al. (2013). Plasma lipid profiling in a large population-based cohort. J. Lipid Res. *54*, 2898–2908.

STAR★METHODS

KEY RESOURCES TABLE

REAGENT or RESOURCE	SOURCE	IDENTIFIER
Antibodies		
PKCε	Becton Dickinson	#610086; RRID: AB_397493
Insulin receptor beta subunit 4B8	Cell Signaling Technology	#3025; RRID: AB_2280448
Phospho-Akt (Ser473)	Cell Signaling Technology	#9271; RRID: AB_329825
Phospho-AS160 (Thr642)	Cell Signaling Technology	#8881; RRID: AB_2651042
Phospho-S6 (S235/236)	Cell Signaling Technology	#4858; RRID: AB_916156
Phospho-4E-BP1 (T37/46)	Cell Signaling Technology	#2855; RRID: AB_560835
Phospho-PRAS40 (Thr246)	Cell Signaling Technology	#2997; RRID: AB_2258110
Beta-Actin	Sigma-Aldrich	A5441, Clone AC-15; RRID: AB_476744
Akt (pan)	Cell Signaling Technology	#4685; RRID: AB_2225340
Sheep anti-mouse IgG HRP-Linked	GE Healthcare	NA931; RRID: AB_772210
Peroxidase AffiniPure Donkey Anti-Rabbit IgG (H+L)	Jackson ImmunoResearch	711-035-152; RRID: AB_10015282
Chemicals, Peptides, and Recombinant Proteins		
Insulin (Actrapid 100 IU/ml))	Novo Nordisk	1331415
Deoxy-D-glucose, 2-[1-14C]	PerkinElmer	NET331A005MC
Deoxy-D-glucose, 2-[1-14C]	PerkinElmer	NEC495A001MC
AG 1-X8	Bio-Rad	140-1443
Bovine serum albumin, fatty acid free	Sigma-Aldrich	A7030
Protein G dynabeads	Thermo Fisher Scientific	10003D
Recombinant protein kinase C epsilon	Burchfield et al., 2004	N/A
Phosphatidyl-L-serine	Sigma-Aldrich	P7769
1,2-dioctanoyl-sn-glycerol	Sigma-Aldrich	D5156
Acetonitrile LC-MS grade	Thermo Fisher Scientific	51101
Tris(2-carboxyethyl)phosphine	Sigma Aldrich	C4706
Chloroacetamide	Sigma-Aldrich	22790
Sequencing grade modified trypsin	Promega	V5111
Empore Styrene Divinyl Benzene (SDB-RPS) 47mm Extraction disks	Supelco Analytical	66886-U
Formic Acid LC-MS grade	Thermo Fisher Scientific	85178
Acetic Acid	Sigma-Aldrich	320099
(-)-Isoproterenol	Sigma-Aldrich	I6504
Mannitol, D-[1-^{14}C]	PerkinElmer	NEC314050UC
Deoxy-D-glucose, 2-[1,2-^{3}H(N)]	PerkinElmer	NET549001MC
NucleoSpin RNA	Macherey-Nagel	740955.250
RNA Clean & Concentrator-5	Zymo Research	R1016
TruSeq Stranded mRNA Library Prep Kit	Illumina	RS-122-2101
Collagenase D	Roche Diagnostics	11088866001
Dispase II	Sigma-Aldrich	D4693
Adenosine	Sigma-Aldrich	A9251
(-)-N6-(R-phenylisopropyl)-adenosine	Sigma-Aldrich	P4532
Adenosine deaminase	Roche Diagnostics	10102121001
Guanidine hydrochloride	Sigma-Aldrich	G4505
2,2,2-Trifluoroethanol	Sigma-Aldrich	96924
Lysyl Endopeptidase mass spectrometry grade	Wako	125-05061
Trifluoroacetic acid LC-MS grade	Thermo Fisher Scientific	85183

(*Continued on next page*)

Continued

REAGENT or RESOURCE	SOURCE	IDENTIFIER
Titanium dioxide beads	GL Sciences	5010-21315
ReproSil-Pur 120 C18, 1.9 mm	Dr. Maisch GmbH HPLC	R119.aq
Critical Commercial Assays		
BCA protein assay kit	Pierce	23227
NEFA-C assay kit	Wako	WA279-75401
Free glycerol assay	Abcam	AB65337
L-alanine assay kit	Abcam	AB83394
TaqMan Reverse Transcription Kit	Thermo Fisher Scientific	N8080234
Deposited Data		
RNA-seq data from adipose tissue and liver	GEO repository	GEO: GSE109835
Proteomic data from adipocytes and liver	PRIDE partner repository	PRIDE: PXD010212
Experimental Models: Organisms/Strains		
$PKC\varepsilon^{fl/fl}$	This paper	N/A
$CMV\text{-}Cre^{+/-}/PKC\varepsilon^{fl/fl}$	This paper	N/A
$Alb\text{-}Cre^{+/-}/PKC\varepsilon^{fl/fl}$	This paper	N/A
$Adipoq\text{-}Cre^{+/-}/PKC\varepsilon^{fl/\Delta}$	This paper	N/A
CMV-Cre	Schwenk et al., 1995	N/A
Alb-Cre	Chow et al., 2014	N/A
Adipoq-Cre	Wang et al., 2010	N/A
Oligonucleotides		
See STAR Methods	This paper	N/A
Software and Algorithms		
Multiquant	AB SCIEX	N/A
TrimGalore! V.0.4.0	Babraham Bioinformatics	N/A
STAR aligner (v.2.5.1)	Dobin et al., 2013	N/A
RSEM (v.1.3.0)	Li and Dewey, 2011	N/A
DESeq2	Love et al., 2014	N/A
ToppCluster	Kaimal et al., 2010	N/A
Cytoscape	Shannon et al., 2003	N/A
MaxQuant/Andromeda v.1.6.1.0	Cox and Mann, 2008	N/A
Perseus v.1.6.1.3	Tyanova et al., 2016	N/A
Skyline	Schilling et al., 2012	N/A
DAVID 6.8	Huang da et al., 2009	N/A
StepOnePlus	Applied Biosystems	N/A
StataSE v.9.2	Stata Corporation	N/A
Prism v.7.0d	GraphPad Software	N/A

CONTACT FOR REAGENT AND RESOURCE SHARING

Further information and requests for resources and reagents should be directed to and will be fulfilled by the Lead Contact, Carsten Schmitz-Peiffer (c.schmitz-peiffer@garvan.org.au).

EXPERIMENTAL MODEL AND SUBJECT DETAILS

Mouse Models

Ethical approval for mouse studies was granted by the Garvan Institute/St. Vincent's Hospital Animal Experimentation Ethics Committee, which fulfills all the requirements of the NHMRC and the NSW State Government, Australia (approval numbers 13/22, 16/20). Animals were handled by trained personnel and all procedures carried out in accordance with the Australian code of practice for the care and use of animals for scientific purposes 8th Edition (2013). Mice were communally housed in a temperature controlled room (22±0.5°C) with a 12h light-dark cycle.

Mice bearing PKCε floxed alleles (PKCε$^{fl/+}$) were generated by Ozgene Pty Ltd (Perth, Australia). A PelleNeo (Ozgene) targeting vector was constructed containing exon 1 of the Prkce gene and a Flippase Recognition Target (FRT) site-flanked Phosphoglycerate Kinase (PGK)-neomycin selection cassette, all flanked by loxP sites and 5′ and 3′ homology arms for recombination with mouse genomic DNA. This vector was electroporated into Bruce4 C57BL/6 ES cells and recombinants selected under neomycin and genotyped by Southern blotting. This was carried out using a 5′ probe binding to the + strand from 86161875-86162379, a 3′ probe binding from 86173755-86174278 and a neomycin probe to confirm a single non-random integration.

Albino-C57BL/6 blastocysts were injected with ES cells possessing the correctly recombined construct and transferred to pseudopregnant foster mothers. Chimeric offspring were selected by coat color and mated with albino C57BL/6 mice to produce black-coated mice with germline transmission of the PKCε floxed allele. These animals were screened for the targeted floxed allele by Southern blot analysis of genomic DNA obtained from tail biopsies. The PGK-neomycin cassette was removed by crossing the wt/PKCε-PGK-Neo-flox mice with C57BL/6 FLPe deleter mice (Brink laboratory, Garvan Institute).

To generate mice with a global deletion of PKCε, we crossed PKCε$^{fl/+}$ mice with transgenic C57BL/6 mice expressing Cre under the control of a human cytomegalovirus (CMV) promoter (CMV-cre^{+}) kindly provided by Frederic Sierro, Garvan Institute (Schwenk et al., 1995) and continued breeding to generate PKCε$^{fl/fl}$ mice with or without the CMV-Cre transgene. Littermate controls also included wildtype mice and CMV-Cre^{+} mice. Similarly, we generated mice with a liver-specific deletion of PKCε, by crossing PKCε$^{fl/+}$ mice with transgenic C57BL/6 mice expressing Cre under the control of a rat albumin promoter (Alb-Cre^{+}) kindly provided by David James, Garvan Institute (Chow et al., 2014). In each case littermate controls also included wildtype mice and respective Cre^{+} mice.

We also generated mice with whole adipose-specific deletion of PKCε using transgenic C57BL/6 mice expressing Cre under the control of a mouse adiponectin promoter (Adipoq-Cre^{+}) kindly provided by Philipp Scherer, University of Texas Southwestern Medical Center (Wang et al., 2010). This led to frequent germline deletion of PKCε in a heterozygous (PKCε$^{fl/\Delta}$) or occasionally homozygous (PKCε$^{\Delta/\Delta}$) manner, as previously reported for aP2-Cre-driven adipose-tissue-specific transgenic mice (Lee et al., 2013). Such deletion was detected through additional genotyping PCR reactions (Figure S2A), and we used it to advantage by including littermate whole-body PKCε-deficient PKCε$^{\Delta/\Delta}$ mice in key experiments. Homozygous PKCε$^{fl/fl}$, adipoq-cre^{+} mice were relatively rare and were reserved for breeding.

PCR genotyping was performed with the following primers:
PKCεf (testing for floxed exon 1) Fw: GTCCTTGGAGAGACACGTGGAGCTC
PKCεf (testing for floxed exon 1) Rv: GGGGCTTCCTACCAGAAAGACGGC
ConDel (testing for deleted exon 1) Fw: CATGCACTCGCTGAGAATC
ConDel (testing for deleted exon 1) Rv: CCTATCACCACAAGCCCTTTTGAG
Cre Fw: CCGGTCGATGCAACGAGTGAT
Cre Rv: ACCAGAGTCATCCTTAGCGCC

METHOD DETAILS

Mouse Diet Feeding

Mice were group-housed (2-5 mice per cage) and fed a standard chow diet (10.88 kJ/g; 8% fat, 21% protein and 71% carbohydrate; Gordon's Specialty Stock Feeds, Yanderra, NSW, Australia). At 8-10 weeks of age, littermates were assigned randomly to either the chow diet (10.88 kJ/g; 8% fat, 21% protein and 71% carbohydrate; Gordon's Specialty Stock Feeds, Yanderra, NSW, Australia) or a lard-based high-fat diet prepared in-house (19.67 kJ/g; 45% fat, 20% protein and 35% carbohydrate [16% sucrose]; based on Research Diets D12451, New Brunswick, NJ, USA) for up to 17 weeks. Mouse body composition was measured by NMR using a EchoMRI-900 Analyzer according to the manufacturer's instructions.

Intraperitoneal Glucose Tolerance Test (ipGTT)

Mice were fasted for 6 h (0800 – 1400) weighed and basal blood samples taken from the tail tip. They were injected intraperitoneally with a 50% glucose solution (2 or 0.5 g/kg body weight for 1 week or 16 week diets respectively) and further blood samples taken at 15, 30 and 45 min. Glucose concentrations were measured using an Accu-Chek Performa glucometer (Roche) at 7.5, 15, 22.5, 30, 45, 60 and 90 min. EDTA (18 mM in saline, 1/3 volume) was added to blood samples which were kept on ice until plasma was obtained by centrifugation at 17,000 g for 1 min. Insulin was measured in mouse plasma by ELISA (CrystalChem). Free fatty acids were assayed in mouse plasma using the NEFA C kit (Wako Diagnostics).

Hyperinsulinemic-Euglycemic Clamps

At 8 weeks of age, dual cannulation surgery was performed under general anaesthesia (4% isoflurane for induction; 1.5-2% maintenance) and aseptic conditions. Catheters were inserted into the left carotid artery and right jugular vein (Brandon et al., 2016). Animals were then left to recover with weights monitored and catheters flushed every 1-2 days. 5-7 days post surgery, a hyperinsulinemic-euglycemic clamp was be performed (Brandon et al., 2016; Ayala et al., 2006). After a 5 h fast, animals received a [3-^{3}H]-glucose (0.05 μCi/min) infusion for 90 min. This allowed the calculation of basal hepatic glucose production and whole body glucose uptake. The hyperinsulinemic clamp was then initiated with a primed-continuous infusion of insulin (16 mU/kg bolus followed by 4 mU/kg/min) and the rate of [3-^{3}H]-glucose infusion was increased to 0.1 μCi/min. Euglycemia (8mM) was maintained during the clamp by measuring blood glucose every 10 min and infusing 25% dextrose as necessary. A bolus of 10 μCi of 2[^{14}C]-deoxyglucose

was administered after euglycemia was established for determination of tissue specific glucose uptake. At the end of the clamp animals were euthanized and tissues collected and stored at -80°C for subsequent analysis. The rate of basal and clamp glucose disappearance (R_d) was determined using steady-state equations. Clamp hepatic glucose output was determined by subtracting the glucose infusion rate (GIR) from R_d. For determination of tissue glucose uptake, tissue samples were homogenized in water. After centrifugation, one aliquot was counted to determine total 2[^{14}C]DG and 2[^{14}C]DGP radioactivity. Another aliquot was run through a column of AG 1-X8 resin (Bio-Rad Laboratories, CA, USA) which retains 2[^{14}C]DGP and elutant containing 2[^{14}C]DG was counted. 2[^{14}C]DGP_{tissue} is the difference between total ^{14}C and 2[^{14}C]DG measures. Using this 2[^{14}C]DGP_{tissue}, glucose uptake into tissues was determined via the following equation:

$$Rg' = (2[^{14}C]DGP_{tissue} / \text{AUC } 2[^{14}C]DG_{plasma})^* \text{ [arterial glucose]}$$

where 2[^{14}C]DGP_{tissue} is the 2[^{14}C]DGP radioactivity in the muscle (in dpm/g), AUC 2[^{14}C]DG_{plasma} is the area under the plasma 2[^{14}C]DG disappearance curve (in dpm/min/ml), and [arterial glucose] is the average blood glucose (in mmol/l) (Ayala et al., 2006).

Immunoblotting

Tissue samples, frozen and powdered under N_2(l), were extracted in RIPA buffer (liver, 50 mg in 250 μl; adipose tissue, 150 mg in 750 μl) with the edition of Complete protease inhibitor cocktail (Roche) and phosphatase inhibitors (10 mM NaF, 1 mM Na_2VO_3). After incubation on ice for 20 min, samples were centrifuged at 17,000 g for 10 min at 4°C. Supernatants were assayed for protein concentration by BCA assay (Pierce) and equal quantities (20 - 50 μg) mixed with NuPAGE LDS 4x sample buffer and 10x reducing agent (Thermo Fisher). Adipocyte extracts were prepared as described for phosphoproteomics below. All protein samples were subjected to SDS-PAGE after heating at 70°C for 10 min, using NuPAGE gradient gels (Thermo Fisher) and buffer systems appropriate for the M_r of the proteins under investigation. Proteins in gels were electrotransferred to Immobilon P PVDF membranes (Millipore) using a Trans-Blot Cell (BioRad) and Tris-glycine buffer containing 20% methanol (v/v). Membranes were blocked for 1 h at room temperature with Tris-buffered saline, 0.05% Tween 20 (TTBS) containing 5% (w/v) bovine serum albumin (BSA). Membranes for analysis of insulin signaling were cut into strips according to M_r and all membranes incubated with primary antibodies in TTBS/BSA for 2 h at room temperature or overnight at 4°C. After washing in TTBS, membranes were further incubated with secondary antibodies conjugated to horseradish peroxidase for 1 h at room temperature. Images were developed using Western Lightning Plus chemiluminescent substrate (Perkin-Elmer) and exposed to X-OMAT Blue XB Film (Kodak) or imaged on a Chemidoc Touch (BioRad). Images on film were scanned with a Epson Perfection V800 Photo scanner and Photoshop CS5.1 software.

Release of Free Fatty Acids and Gluconeogenic Substrates from Adipose Tissue Explants

Gonadal fat pads were harvested from 1 week fat-fed female mice, rinsed in saline and transferred to 2 ml serum-free DMEM containing 5 mM glucose, 25 mM Hepes pH 7.4 and 2% BSA at 37°C. Pads dissected into approximately 30 mg explants and preincubated for 2 h in fresh DMEM. Individual explants were washed twice and incubated for 1 hr in 500 μl Krebs-Ringer Phosphate (KRP) buffer with 5mM glucose, 25 mM Hepes pH 7.4 and 3.5% BSA at 37°C. Further additions of 5 nM isoproterenol, 100 nM insulin or 25 mM glucose were as stated in figure legends. Following the incubations, explants were removed, gently blotted and weighed, and the release of free fatty acids and the gluconeogenic substrates glycerol and alanine into the KRP buffer was determined using spectrophotometric assay kits according to the manufacturers' instructions (Wako NEFA-C kit, Abcam free glycerol and L-alanine assay kits). Lactate was assayed using a fluorometric adaptation of the method of Gutmann and Wahlefeld (Gutmann and Wahlefeld, 1974) after KRP buffer was deproteinized with 6% $HClO_4$ and neutralised with 5M NaOH.

Glucose Transport in Adipose Tissue Explants

Explants were prepared and preincubated for 2 h as described above for measurement of fatty acid release. Explants were then washed twice and incubated in 475 μl KRP with 25 mM Hepes pH 7.4 and 3.5% BSA at 37°C for 15 min in the absence or presence of 100 nM insulin. After the addition of 25 μl KRP with 100 μM 2-deoxyglucose, 10 μCi [^{3}H]2-deoxyglucose and 2 μCi [^{14}C]mannitol, explants were incubated for a further 20 min before transfer to glass filters on a vacuum manifold. Explants were washed four times with ice-cold PBS, weighed and homogenized in 200 μl RIPA buffer. After centrifugation at 17,000 g at 4°C for 10 min, 100 μl infranatant was mixed with 4 ml scintillation cocktail and tracer uptake determined by dual-label beta-counting. 2-deoxyglucose uptake was corrected for extracellular tracer using mannitol recovery.

Lipid Analysis

Triacylglycerol, diacylglycerol, sphingolipid, cholesterol esters and phospholipid species were measured as previously described (Weir et al., 2013) with minor modifications. Briefly, liver samples were homogenized and sonicated in phosphate buffered saline (PBS) (pH 7.4), a protein assay conducted and 50μg of each sample utilized for lipid extraction. An internal standard mixture and $CHCl_3$/methanol (2:1) were added to each sample before being vortexed, mixed, sonicated, and centrifuged. The lipid-containing supernatant was removed and dried, before the lipids were resuspended in H_2O-saturated butanol then sonicated, before methanol with 10mM ammonium was added. The resuspended samples were centrifuged before the supernatant was transferred to individual glass vials. Lipidomic determination was performed on the samples by liquid chromatography electrospray ionization tandem mass spectrometry combined with triple quadrupole mass spectrometer. Data were analyzed using Multiquant software v1.2 and specific lipid species normalized to the total phosphatidylcholine (PC) levels of each sample.

RNA-Seq Analysis

RNA was extracted from liver using NucleoSpin RNA (Macherey-Nagel) according to the manufacturer's instructions. RNA extraction from gonadal fat pads was performed using Trizol followed by a RNA clean-up using RNA Clean & Concentrator-5 (Zymo Research). Library preparation for RNA-seq was performed using TruSeq Stranded mRNA Library Prep Kit (Illumina). For quality control of the libraries the samples were inspected using a Bioanalyzer chip (DNA 1000, Agilent). Sequencing was performed paired-end on a HiSeq 2500 v4.0 system.

The resulting fastq files were quality controlled using FastQC, adapters were trimmed using TrimGalore! v0.4.0 for paired-end sequenced samples. The trimmed fastq files were aligned to the mouse reference genome (Mus_musculus.GRCm38.85) using STAR aligner (v2.5.1) (Dobin et al., 2013). RSEM (v1.3.0) (Li and Dewey, 2011) was used to estimate gene and isoform expression levels. Downstream analysis for differential gene expression of the raw count table was performed using DESeq2 (Love et al., 2014) in R. Expression levels were considered significantly different between groups when $p < 0.05$ (adjusted for multiple comparisons using Benjamini-Hochberg correction (Benjamini and Hochberg, 1995).

Enrichment term analysis was performed using ToppCluster (Kaimal et al., 2010) and only enrichment terms with p values < 0.05 were considered (adjusted for multiple comparisons using Benjamini-Hochberg correction). Significant enrichment terms were manually selected and curated to avoid repetition of similar terms and the resulting networks manually arranged using Cytoscape (Shannon et al., 2003).

Insulin Receptor Immunoprecipitation, In-gel Protein Digestion and Peptide Extraction

Liver samples were extracted in RIPA buffer as described for immunoblotting and supernatants diluted to 5 mg protein in 500 μl RIPA buffer. Samples were incubated with 10 μl insulin receptor antibody overnight at 4°C on a Nutator (Becton Dickinson). Immunocomplexes were harvested by the addition of 1.5 mg Protein G Dynabeads and incubation for 2 h at 4°C on a Nutator. Beads were washed 3 times in RIPA buffer using a magnetic separation rack (Cell Signaling Technology). For samples phosphorylated *in vitro* with recombinant PKCε, beads were further washed once in 20 mM MOPS pH 7.5. PKCε was prepared as previously described (Burchfield et al., 2004), desalted into PBS using 2 ml Zeba columns (Pierce), diluted to 5 μM and supplemented with 0.5% BSA. Beads were incubated for 20 min at 37°C with 30 μl of 20 mM MOPS, pH 7.5, 1 mM EGTA, 0.04% Triton X-100, 120 μg/ml phosphatidyl-L-serine, 2.5 μg/ml 1,2-dioctanoyl-*sn*-glycerol, 1 μM PKCε, 100 μM ATP, 5 mM $MgCl_2$. The reaction was terminated by washing beads 3 times with RIPA buffer. All beads were resuspended in 35 μl NuPAGE sample buffer with reducing agent, heated at 70°C for 10 min and subjected to SDS-PAGE as above. Gels were fixed in 50% (v/v) methanol, 7.5% (v/v) acetic acid for 30 min, rinsed, and stored in 7.5% acetic acid at 4°C. Proteins were visualized by Sypro Ruby staining overnight and imaged on a Typhoon FLA 9500 (GE Life sciences). SDS-PAGE protein bands were excised and destained in 50% acetonitrile containing 100 mM ammonium bicarbonate. Protein was incubated with 10 mM Tris(2-carboxyethyl)phosphine (TCEP) and 40 mM chloroacetamide containing 100 mM ammonium bicarbonate, pH 7.9 for 30 min at room temperature. SDS-PAGE protein bands were dehydrated and rehydrated in 14 ng/μl of trypsin and digested overnight at 37°C. Peptides were purified by SDB-RPS stage tips and dried by vacuum centrifugation. Mass spectrometry and data analysis were performed as described below.

Primary Adipocyte Isolation, Incubation and Protein Preparation for Proteomic and Phosphoproteomic Analyses

Adipocytes were isolated and incubated as described by Rodbell (Rodbell, 1964), with modifications as suggested by Honnor et al. (Honnor et al., 1985). Perigonadal fat pads were harvested from 10 female chow-fed AdEpsKO mice (12.3 ± 1.0 weeks old) and 10 $PKC\varepsilon^{fl/\Delta}$ littermate control mice (12.4 ± 1.2 weeks old). Pads from 2 mice were combined, minced with scissors and shaken for 40 min at 37°C (200 cycles/s) in 8 ml KRP buffer (pH 7.4) with the addition of 25 mM Hepes, 3.5% BSA, 5 mM glucose, 1 U/ml Collagenase D and 1 U/ml Dispase II, when most tissue had been digested. Cells were filtered through a 250 μm nylon net and washed 3 times with 5 ml KRP buffer with the addition of 25 mM Hepes, 3.5% BSA, 5 mM glucose and 200 nM adenosine, retaining only floating adipocytes while stromal vascular cells were discarded. Adipocytes were preincubated in 5 ml KRP buffer with the addition of 25 mM Hepes, 3.5% BSA, 5 mM glucose, 100 nM (-)-N6-(R-phenylisopropyl)-adenosine (PIA) and 0.5 U/ml adenosine deaminase for 30 min at 37°C with gentle shaking (120 cycles/s). Cells were then divided into 2 incubations with a total volume of 10 ml of the same buffer without or with the addition of 100 nM insulin/30 mM glucose (final concentrations). After incubation for 10 min at 37°C with gentle shaking, buffers were rapidly exchanged for similar buffers containing no BSA and cells further incubated, for a total of 15 min. All buffer was then removed, cells frozen in liquid nitrogen and stored at -70°C.

Cells were subsequently lysed in 100 μl of 6 M guanidine, 10 mM TCEP, 40 mM chloroacetamide and 100 mM Tris, pH 8.5, and lysates heated at 95°C for 5 min and centrifuged at 20,000 g for 30 min, 4°C. Infranatants were diluted 1:1 with MilliQ water and proteins were precipitated by the addition of 4 volumes of ice-cold methanol, 1 volume of ice-cold chloroform and 3 volumes of ice-cold MilliQ water. Suspensions were centrifuged at 9,000 g for 1 min, 4°C and the upper phase discarded. After addition of 3 volumes of ice-cold methanol, proteins were again centrifuged, at 12,000 g for 2 min, 4°C. Protein pellets were washed with 5 volumes of ice-cold methanol and centrifuged at 12,000 x g for 2 min, 4°C. Finally, proteins were resuspended in 200 μl of 10% trifluoroethanol, 100 mM Hepes, pH 7.5 using a BioRuptor. After protein determination by BCA assay, samples were subjected to immunoblotting and also proteomic analysis as below.

Phosphopeptide Enrichment

Phosphoproteomic analysis was performed essentially as described previously (Humphrey et al., 2015). Briefly, protein was digested with Lys-C/trypsin at 1:50 enzyme:substrate ratio overnight at 37°C. The digests were adjusted with final concentrations of 300 mM KCl, 5 mM KH_2PO_4, 50% acetonitrile and 6% Trifluoroacetic acid (TFA), and phosphopeptides bound to titanium dioxide beads at 10:1 beads:peptide ratio (GL Sciences, Japan) at 40°C for 5 min in a ThermoMixer at 2,000 rpm. Non-phosphorylated peptides were removed by washing the beads with 80% acetonitrile containing 6% TFA and eluted with 40% acetonitrile containing 3.75% NH_4OH. Phosphopeptides were purified by SDB-RPS stage tips and dried by vacuum centrifugation.

Mass Spectrometry

Peptides were resuspended in 2% acetonitrile, 0.1% formic acid and loaded onto a 40 cm x 75 μm inner diameter column packed in-house with 1.9 μm C18AQ particles (Dr Maisch GmbH HPLC) using an Easy nLC-1200 UHPLC operated in single-column mode with intelligent flow control loading at 950 bar. Peptides were separated using a linear gradient of 5 – 30% Buffer B over 60 min (for immunoprecipitated insulin receptor and phosphoproteomic analysis) or 180 min (for total proteomic analysis) at 300 nl/min (Buffer A = 0.1% formic acid; Buffer B = 90% acetonitrile, 0.1% acetic acid). The column was maintained at 60°C using a PRSO-V1 ion-source (Sonation) coupled directly to a Q-Exactive HF mass spectrometer (for immunoprecipitated insulin receptor) or a Q-Exactive HFX mass spectrometer (for proteomic and phosphoproteomic analysis). A full-scan MS1 was measured at 60,000 resolution (300 – 1600 m/z; 60 ms injection time; 3e6 AGC target) followed by isolation of up to 7 (HF) or 10 (HFX) most abundant precursor ions for MS/MS (1.2 m/z isolation; 27 normalized collision energy; 15,000 resolution; 60 ms injection time; 1e5 AGC target).

Analysis of Mass Spectrometry Data

All data were processed using MaxQuant/Andromeda (v1.6.1.0) and searched against the Mouse UniProt database (March, 2018) (Cox and Mann, 2008). The data were searched with the following variable modifications; methionine oxidation; serine, threonine, and tyrosine phosphorylation. Carbamidomethylation of cysteine was set as a fixed modification. All search parameters were default and false discovery rate at both the peptide spectral match and protein level set to 1%. Only phosphorylation sites localized by >75% were included in further analysis. Quantification of phosphopeptides immunoprecipitated from the insulin receptor was performed manually with MS1 filtering in Skyline (Schilling et al., 2012). Phosphopeptides from adipocytes were analysed using EasyPhos (Humphrey et al., 2015) resulting in the identification 8,996 unique phosphosites of which 5,829 were quantified in at least 2 biological replicates. Analysis of proteomic and phosphoproteomics data were performed in Perseus (v1.6.1.3) (Tyanova et al., 2016). Differential analysis was performed with t tests and corrected for multiple hypothesis testing with Benjamin Hochberg FDR at q-value <0.1. Functional annotation clustering was performed using DAVD 6.8. Enrichment term analysis by cellular compartment was performed using ToppCluster and only terms with FDR < 0.05 were considered. The resulting network was manually arranged using Cytoscape.

Histology and Adipocyte Size Measurement

Epididymal fat pads from AdEpsKO mice and littermate controls fed a high-fat diet for 16 weeks were fixed in 10% neutral-buffered formalin for 24 h and stored in 70% ethanol. Tissues were embedded in paraffin, sectioned at 4 μm and stained with hematoxylin and eosin (H&E). Slides were imaged with a Leica DM4000 microscope using a ×20 objective. Adipocyte cell sizes were measured in 3 images per mouse with ImageJ using the Adipocyte Tools plugin.

Quantitative Real-Time-PCR (qRT-PCR)

Tissues were harvested from mice fasted as for ipGTT, frozen and powdered under N_2(l). RNA was isolated from 50 mg of liver as for RNA-seq. 450-1150ng of RNA was reversed-transcribed to generate cDNA using the TaqMan Reverse Transcription Kit (Thermo Fisher) as per manufacturer's instructions. qRT-PCR was carried out using the Universal Probe Library (UPL) system on a LightCycler 480 (Roche). The primers used for specific genes are listed below. Data were analyzed using StepOnePlus (Applied Biosystems). Standard curves were constructed for each gene to confirm amplification efficiency. Quantification was calculated using the ΔΔCt method, with differences in cDNA input corrected by normalizing signals obtained with specific primers for housekeeping genes (TATA box binding protein or cyclophilin A for adipose tissue and liver respectively).

Primer Sequences and UPL Probe Numbers
Ahsg
Ahsg.UPL62.F gtcacagatccagccaaatg
Ahsg.UPL62.R tgagatttgccttgcagaag
ApoA1
Apoa1.UPL63.F caaagacagcggcagagact
Apoa1.UPL63.R cccagagtgtcccagttttc
Cebpb
Cebpb.UPL102.F tgatgcaatccggatcaa
Cebpb.UPL102.R cacgtgtgttgcgtcagtc
H19

H19.UPL42.F ggtgtgatggagaggacagaa
H19.UPL42.R agacggcttctacgacaagg
Hamp
Hamp.UPL64.F gatggcactcagcactcg
Hamp.UPL.64R ctgcagctctgtagtctgtctca
Lpl
Lpl.UPL47.F tttgtgaaatgccatgacaag
Lpl.UPL47.R cagatgctttcttctcttgtttgt

QUANTIFICATION AND STATISTICAL ANALYSIS

Results are shown as means ± SEM of independent experiments. Statistical tests and experimental numbers are detailed in figure legends. Factorial ANOVA and t tests were performed using StataSE v9.2 (Stata Corporation, TX, USA) or Prism v7.0d (Graphpad Software, CA, USA).

DATA AND SOFTWARE AVAILABILITY

The mass spectrometry total and phospho-proteomics data have been deposited to the ProteomeXchange Consortium via the PRIDE partner repository with the dataset identifier PXD010212.

The RNA-seq data have been deposited in the GEO repository under ID code GSE109835.